Comput. Methods Appl. Mech. Engrg. 198 (2008) 397–406

Contents lists available at ScienceDirect

Comput. Methods Appl. Mech. Engrg.

journal homepage: www.elsevier.com/locate/cma

Numerical homogenization of the acoustic wave equations with a continuum of scales

Houman Owhadi [a], Lei Zhang [b,*]

[a] California Institute of Technology Applied & Computational Mathematics, Control & Dynamical Systems, MC 217-50 Pasadena, CA 91125, United States
[b] California Institute of Technology Applied & Computational Mathematics, MC 217-50 Pasadena, CA 91125, United States

A R T I C L E I N F O

Article history:
Received 12 November 2007
Received in revised form 1 June 2008
Accepted 15 August 2008
Available online 2 September 2008

MSC:
Primary 35L05, 35B27
Secondary
65M15, 86-08, 74Q15

Keywords:
Multi-scale problem
Compensation
Numerical homogenization
Upscaling
Acoustic wave equation

A B S T R A C T

In this paper, we consider numerical homogenization of acoustic wave equations with heterogeneous coefficients, namely, when the bulk modulus and the density of the medium are only bounded. We show that under a Cordes type condition the second order derivatives of the solution with respect to harmonic coordinates are L^2 (instead H^{-1} with respect to Euclidean coordinates) and the solution itself is in $L^\infty(0,T,H^2(\Omega))$ (instead of $L^\infty(0,T,H^1(\Omega))$ with respect to Euclidean coordinates). Then, we propose an implicit time stepping method to solve the resulted linear system on coarse spatial scales, and present error estimates of the method. It follows that by pre-computing the associated harmonic coordinates, it is possible to numerically homogenize the wave equation without assumptions of scale separation or ergodicity.

1. Introduction

Let Ω be a bounded and convex domain of class C^2 of $\mathbb{R}^2$. Let $T>0$. Consider the following acoustic wave equation

$$\begin{cases} K^{-1}(x)\partial_t^2 u = \operatorname{div}(\rho^{-1}(x)\nabla u(x,t)) + g \quad \text{in } \Omega\times(0,T). \\ u(x,t)=0 \quad \text{for } (x,t)\in\partial\Omega\times(0,T). \\ u(x,t)=u(x,0) \quad \text{for } (x,t)\in\Omega\times\{t=0\}. \\ \partial_t u(x,t)=u_t(x,0) \quad \text{for } (x,t)\in\Omega\times\{t=0\}. \end{cases} \tag{1.1}$$

Write $\Omega_T := \Omega\times(0,T)$ and $a:=\rho^{-1}$. We assume a is a uniformly elliptic 2×2 symmetric matrix on $\overline{\Omega}$ whose entries are bounded and measurable. There exists $0<a_{\min}\leqslant a_{\max}$, such that $\forall\xi\in\mathbb{R}^2$, $|\xi|=1$, $a_{\min}\leqslant {}^t\xi a(x)\xi\leqslant a_{\max}$, $\forall x\in\Omega$. K is a scalar such that $K_{\min}\leqslant K\leqslant K_{\max}$. $g\in L^2(\Omega_T)$.

Eq. (1.1) can be used to model wave propagation in heterogeneous media. It is important in many applications such as geophysics, seismology, and electromagnetics [6,9,31,33]. In geophysical and seismic prospecting, K stands for the bulk modulus, ρ the density and u the unknown pressure. The velocity c and acoustic impedance σ are given by $c=\sqrt{K/\rho}$ and $\sigma=\sqrt{K\rho}$.

Wave propagation in heterogeneous media involves many different spatial scales. Even with modern state-of-the-art supercomputers, a direct simulation of the highly heterogeneous media is often difficult if not impossible. That is why we want to use multi-scale methods to solve (1.1) on the coarse spatial scales. More precisely, we want to know how to transfer information from fine scales to coarse scales, and how to use the information obtained to solve the coarse scale problem with much fewer degrees of freedom. We often refer this procedure as numerical homogenization or numerical upscaling.

The idea of using oscillating test functions in relation to homogenization can be backtracked to the work of Murat and Tartar on homogenization and H-convergence, in particular we refer to [27,32] (recall also that the framework of H-convergence is independent from ergodicity or scale separation assumptions). The implementation and practical application of oscillating test functions in finite element based numerical homogenization have been called multi-scale finite element methods (MsFEM) and have been studied by numerous authors [3,7,13,16,21]. On the other hand, numerical schemes have been developed to solve the acoustic wave equation with discontinuous coefficients, for example in [9] by nonconforming finite element method and in [6] by domain

* Corresponding author. Current address: Max Planck Institute for Mathematics in Sciences, Leipzig, 04103, Germany.
E-mail addresses: owhadi@caltech.edu (H. Owhadi), zhanglei@acm.caltech.edu (L. Zhang).

0045-7825/$ - see front matter © 2008 Elsevier B.V. All rights reserved.
doi:10.1016/j.cma.2008.08.012

decomposition. Recently, numerical homogenization or numerical upscaling methods such as [33] are proposed for wave equation with heterogeneous coefficients.

The finite element method in this paper is closer in spirit to the work of Hou and Wu [21] and Allaire and Brizzi [3]. It is based on a technique first introduced in [29] for elliptic equations and extended in [28] to parabolic equations characterised by a continuum of scales in space and time. The main difference lies in the fact that, instead of solving a local cell problem to get a basis function as in MsFEM (Multi-scale finite element method) or to calculate effective media property as in upscaling method [15], we use a global change of coordinates. The global change of coordinates allows to avoid the so called cell resonance problem and obtain a scheme converging in situations where the medium has no separation between scales. This makes our method amenable to problems with strongly non-local medias, such as high conductivity channels.

We use a composition rule to construct the finite element space. I. Babuška et al. introduced the so called "change of variable" technique [7] in the general setting of partition of unity method (PUM) with p-version of finite elements. Through this change of variable, the original problem is mapped into a new one which can be better approximated. Allaire and Brizzi [3] introduced the composition rule in the multi-scale finite element formulation, and have observed that a multi-scale finite element method with higher order Lagrange polynomials has a higher accuracy.

The main difference with parabolic equations [28] lies in the fact that with hyperbolic equations, energy is conserved and after homogenization there is no hope of recovering the energy (or information) lying in the highest frequencies. However when the medium is highly heterogeneous the eigenfunctions associated to the highest frequencies are localized, thus energy is mainly transported by the lowest frequencies. That is why, when one is only interested in the large scale transport of energy it is natural to approximate the solutions of (1.1) by the solutions of an homogenized operator. For localization of waves in heterogeneous media, we refer to [4,24,30].

This paper is organized as follows. In the next section, we present the formulation of the mathematical problem and numerical methods, and also show main results. In Section 3, we will give the detailed proof and explanation of the results in Section 2. In Section 4, we present several numerical examples and conclusions.

2. Main results

In general, the approximation power of finite element method is subject to the best approximation for an exact solution with respect to the finite element space. Therefore, we require smoothness of the solution to prove convergence theorems. That is one of the reasons why standard methods are not applicable for problems with heterogeneous media. For example, in (1.1), we only have $u \in L^\infty(0,T,H^1(\Omega))$, and we can not gain anything if we approximate the solution with usual C^0 or C^1 finite element basis. However, as in [29], we can find harmonic coordinates which the solution of the wave equation is smoothly dependent on, which is the so-called compensation phenomena.

2.1. Compensation phenomena

We will focus on space dimension $n=2$. The extension to higher dimension is straightforward conditioned on the stability of σ. Let $F := (F_1, F_2)$ be the harmonic coordinates satisfying

$$\begin{cases} \operatorname{div} a\nabla F = 0 & \text{in } \Omega, \\ F(x) = x & \text{on } \partial\Omega. \end{cases} \tag{2.1}$$

Let $\sigma := {}^t\nabla F a \nabla F$ and

$$\mu_\sigma := \operatorname{esssup}_{x\in\Omega}\left(\frac{\lambda_{\max}(\sigma(x))}{\lambda_{\min}(\sigma(x))}\right). \tag{2.2}$$

Condition 2.1. σ satisfies Cordes type condition if: $\mu_\sigma < \infty$ and $(\mathrm{Trace}[\sigma])^{-1} \in L^\infty(\Omega)$.

Remark 2.1. If F is a quasiregular mapping, i.e., the dilation quotient (the ratio of maximal to minimal singular values of the Jacobi matrix) is bounded, Cordes type Condition 2.1 is satisfied [2]. An invertible quasiregular mapping is called quasiconformal. In [2] and references therein, invertibility of F is proved for $a \in L^\infty(\Omega)$. Some sufficient conditions for F being quasiconformal were also given, for example, $\det(a)$ is locally Hölder continuous. Unfortunately, a counterexample with checkerboard structure was proposed, and it can be shown that μ_σ is unbounded at the intersecting point, which is known in mechanics as stress concentration. However, we will show that as a solution technique, the numerical methods proposed in this paper also works for the cases with stress concentration.

Let $L^2(0,T;H_0^1(\Omega))$ be the Sobolev space associated to the norm

$$\|v\|^2_{L^2(0,T;H_0^1(\Omega))} := \int_0^T \|v(\cdot,t)\|^2_{H_0^1(\Omega)}\,\mathrm{d}t. \tag{2.3}$$

Also, we define the norm of the space $L^\infty(0,T,H^2(\Omega))$ by

$$\|v\|_{L^\infty(0,T,H^2(\Omega))} = \operatorname{esssup}_{0\leqslant t\leqslant T}\left(\int_\Omega \sum_{i,j}(\partial_i\partial_j v(x,t))^2\,\mathrm{d}x\right)^{\frac{1}{2}}. \tag{2.4}$$

We require the right hand side g, initial value $u(x,0)$ and $u_t(x,0)$ to be smooth enough, which is a reasonable assumption in many applications. For example, we can made the following assumptions:

Assumption 2.1. Assume that the g satisfies $\partial_t g \in L^2(\Omega_T)$, $g \in L^\infty(0,T,L^2(\Omega))$, initial data $u(x,0)$ and $\partial_t u(x,0)$ satisfy $\partial_t u(x,0) \in H^1(\Omega)$ and $\nabla a(x)\nabla u(x,0) \in L^2(\Omega)$ or equivalently $\partial_t^2 u(x,0) \in L^2(\Omega)$.

We have the following compensation theorem:

Theorem 2.1. *Suppose that Cordes Condition 2.1 and Assumption 2.1 hold, then $u \circ F^{-1} \in L^\infty(0,T,H^2(\Omega))$ and*

$$\|u\circ F^{-1}\|_{L^\infty(0,T,H^2(\Omega))} \leqslant C(\|g\|_{L^\infty(0,T,L^2(\Omega))} + \|\partial_t g\|_{L^2(\Omega_T)} + \|\partial_t u(x,0)\|_{H^1(\Omega)} + \|\partial_t^2 u(x,0)\|_{L^2(\Omega)}). \tag{2.5}$$

The constant C can be written as

$$C = C(n,\Omega,K_{\min},K_{\max},a_{\min},a_{\max})\mu_\sigma\|(\mathrm{Trace}[\sigma])^{-1}\|_{L^\infty(\Omega)}. \tag{2.6}$$

Remark 2.2. We have gained one more order of integrability in the harmonic coordinates since in general $u \in L^\infty(0,T,H^1(\Omega))$. The condition $g \in L^2(\Omega_T)$ is sufficient to obtain Theorem 2.1 and the following theorems. For the sake of clarity we have preferred to restrict ourselves to $g \in L^\infty(0,T,L^2(\Omega))$.

2.2. Numerical homogenization in space

Suppose we have a quasiuniform mesh. Let X^h be a finite dimensional subspace of $H_0^1(\Omega)\cap W^{1,\infty}(\Omega)$ with the following approximation properties: There exists a constant C_X such that

- Interpolation property, i.e., for all $f \in H^2(\Omega)\cap H_0^1(\Omega)$

$$\inf_{v\in X^h}\|f-v\|_{H_0^1(\Omega)} \leqslant C_X h\|f\|_{H^2(\Omega)}. \tag{2.7}$$

- Inverse Sobolev inequality, i.e., for all $v \in X^h$

$$\|v\|_{H^2(\Omega)} \leqslant C_X h^{-1}\|v\|_{H_0^1(\Omega)} \tag{2.8}$$

and

$$\|v\|_{H_0^1(\Omega)} \leqslant C_X h^{-1}\|v\|_{L^2(\Omega)}. \tag{2.9}$$

These properties are known to be satisfied when X^h is a C^1 finite element space. One possibility is to use weighted extended B-splines (WEB) method developed by Höllig in [19,20], these elements are in general C^1-continuous. They are obtained from tensor products of one dimensional B-spline elements. The homogeneous Dirichlet boundary condition is satisfied by multiplying the basis functions with a smooth weight function ω which satisfies $\omega = 0$ at the boundary.

Write the solution space V^h as

$$V^h := \{\varphi \circ F(x) : \varphi \in X^h\}. \tag{2.10}$$

Remark 2.3. We prove all the following theoretical results using exact F, however, in the numerical implementations, we have to compute a discrete solution $F_{h'}$ on a fine mesh of size h' to approximate F. We always assume that $h' \ll h$, namely, h' is the size of fine mesh and h is the size of coarse mesh. In [3], Allaire and Brizzi proved the convergence of multi-scale finite element method with respect to the discrete map $F_{h'}$ in the periodic case using asymptotic expansion, as well as some regularity assumptions requiring the mappings F and $F_{h'}$ smooth enough. However, in the general case, neither the tool of asymptotic expansion nor smoothness assumption is available, which makes a complete justification more difficult. Some discussions and further suggestions for similar problems in the context of variational mesh generation can be found in [18]. Another problem is, although F is guaranteed to be invertible, $F_{h'}$ is not. Fortunately, this can be relieved if F is solved by piecewise linear finite element and the mesh only has non-obtuse-angled triangles [17].

We use the following notation:

$$a[v,w] := \int_\Omega {}^t\nabla v(x,t)a(x)\nabla w(x,t)\mathrm{d}x. \tag{2.11}$$

For $v \in H_0^1(\Omega)$ write $\mathscr{R}_{h,0}v$ the Ritz–Galerkin projection of v on V^h with respect to the bilinear operator $a[\cdot,\cdot]$, i.e., the unique element of V^h such that for all $w \in V^h$,

$$a[w, v - \mathscr{R}_{h,0}v] = 0. \tag{2.12}$$

Define Y_T^h the subspace of $L^2(0,T;H_0^1(\Omega))$ as

$$Y_T^h := \{v \in L^2(0,T;H_0^1(\Omega)) : v(x,t) \in V^h, \ \ \forall t \in [0,T]\}. \tag{2.13}$$

Write u_h the solution in Y_T^h of the following system of ordinary differential equations:

$$\begin{cases} (K^{-1}\psi(x), \partial_t^2 u_h)_{L^2(\Omega)} + a[\psi(x), u_h] \\ \quad = (\psi(x), g)_{L^2(\Omega)} \quad \forall t \in (0,T) \quad \text{and} \quad \psi \in V^h, \\ u_h(x,0) = \mathscr{R}_{h,0}u(x,0), \\ \partial_t u_h(x,0) = \mathscr{R}_{h,0}\partial_t u(x,0). \end{cases} \tag{2.14}$$

The following theorem shows the error estimate of the semi-discrete solution. We need more smoothness on the forcing term g and the initial data than Assumption 2.1 to guarantee the $O(h)$ convergence of the scheme (2.14). On the other hand, we can see that even if g and all the initial data are smooth, with general conductivity matrix $a(x)$, we can merely expect $u \in L^\infty(0,T,H^1(\Omega))$ instead of the improved regularity $L^\infty(0,T,H^2(\Omega))$ in the harmonic coordinates, and the convergence rates will deteriorate for the conventional finite elements.

Assumption 2.2. Assume that the forcing term g satisfies $\partial_t^2 g \in L^2(\Omega_T)$, $\partial_t g \in L^\infty(0,T,L^2(\Omega))$, initial value $u(x,0)$ and $\partial_t u(x,0)$ satisfy $\partial_t^2 u(x,0) \in H^1(\Omega)$ and $\nabla a(x)\nabla\partial_t u(x,0) \in L^2(\Omega)$ or equivalently $\partial_t^3 u(x,0) \in L^2(\Omega)$.

From now on we will always suppose without explicitly mentioning that Assumption 2.2 is satisfied in the discussion of numerical homogenization method.

Theorem 2.2. *Suppose that Cordes Condition 2.1 and Assumption 2.2 hold, we have*

$$\begin{aligned} &\|\partial_t(u-u_h)(\cdot,T)\|_{L^2(\Omega)} + \|(u-u_h)(\cdot,T)\|_{H_0^1(\Omega)} \\ &\leqslant Ch(\|\partial_t g\|_{L^\infty(0,T,L^2(\Omega))} + \|\partial_t^2 g\|_{L^2(\Omega_T)} + \|\partial_t^2 u(x,0)\|_{H^1(\Omega)} \\ &\quad + \|\partial_t^3 u(x,0)\|_{L^2(\Omega)}). \end{aligned} \tag{2.15}$$

The constant C depends on C_X, n, Ω, μ_σ, $K_{\min}$, $K_{\max}$, $a_{\min}$, $a_{\max}$, and $\|(Trace[\sigma])^{-1}\|_{L^\infty(\Omega)}$.

Remark 2.4. In the numerical implementation, the real solution space is $V^{h,h'} := \{\varphi \circ F_{h'}(x) \ \varphi \in X^h\}$. Let $u_{h,h'}$ be the solution of (2.14) with the solution space V^h replaced by $V^{h,h'}$. The error analysis for $u - u_{h,h'}$ can be made separately for two parts, $u - u_h$ and $u_h - u_{h,h'}$. We can use a perturbation argument to estimate $u_h - u_{h,h'}$. Suppose that $\|\varphi\circ F - \varphi \circ F_{h'}\| \to 0$ as $h' \to 0$, the norm $\|\cdot\|$ can be taken as, for example, L^∞ norm. In view of the inequality $\|\varphi \circ F - \varphi\circ F_{h'}\| \leqslant \sup|D\varphi|\|F - F_{h'}\|$, it is equivalent to $\|F - F_{h'}\| \to 0$ as $h' \to 0$ for fixed coarse space X^h. Now the ODE system corresponding to $u_{h,h'}$ is a perturbation of the ODE system corresponding to u_h, $u_h - u_{h,h'}$ can be controlled by a Gronwall inequality [10]. Note this is just a sketch and a complete proof will be done elsewhere.

2.3. Numerical homogenization in time and space

Let $M \in \mathbb{N}$, $(t_n = n\frac{T}{M})_{0\leqslant n\leqslant M}$ is a discretization of $[0,T]$. (φ_i) is a C^1 basis of X^h. Write trial space Z_T^h the subspace of Y_T^h such that

$$Z_T^h = \left\{ w \in Y_T^h : w(x,t) = \sum_i c_i(t)\varphi_i(F(x)), \ \ c_i(t) \right.$$
$$\left. \times \text{are linear on } (t_n, t_{n+1}] \text{ and continuous on } [0,T] \right\}. \tag{2.16}$$

Let test space U_T^h be the subspace of Y_T^h such that

$$U_T^h = \left\{ \psi \in Y_T^h : \psi(x,t) = \sum_i d_i\varphi_i(F(x)), \ \ d_i \text{ are constant on } [0,T] \right\}. \tag{2.17}$$

Write v_h the solution in Z_T^h of the following system of implicit weak formulation: for $n \in \{0,\ldots,M-1\}$ and $\psi \in U_T^h$

$$\begin{aligned} &(K^{-1}\psi, \partial_t v_h)(t_{n+1}) - (K^{-1}\psi, \partial_t v_h)(t_n) \\ &\quad = \int_{t_n}^{t_{n+1}} (K^{-1}\partial_t\psi, \partial_t v_h)\mathrm{d}t - \int_{t_n}^{t_{n+1}} a[\psi, v_h]\mathrm{d}t + \int_{t_n}^{t_{n+1}} (\psi, g)\mathrm{d}t. \end{aligned} \tag{2.18}$$

In Eq. (2.18), $\partial_t v_h(t)$ stands for $\lim_{\epsilon\downarrow 0}(v_h(t) - v_h(t-\epsilon))/\epsilon$. Once we know the values of v_h and $\partial_t v_h$ at t_n, (2.18) is a linear system for the unknown coefficients of $\partial_t v_h(t_{n+1})$ in V^h. By continuity of v_h in time, we can obtain $v_h(t_{n+1})$ by

$$v_h(t_{n+1}) = \partial_t v_h(t_{n+1})(t_{n+1} - t_n) + v_h(t_n). \tag{2.19}$$

The following Theorem 2.3 shows the stability of the implicit scheme (2.18):

Theorem 2.3. *Suppose that Cordes Condition 2.1 and Assumption 2.2 hold, we have*

$$\begin{aligned} &\|\partial_t v_h(\cdot,T)\|_{L^2(\Omega)} + \|v_h(\cdot,T)\|_{H_0^1(\Omega)} \\ &\leqslant C(\|g\|_{L^2(\Omega_T)} + \|\partial_t u(x,0)\|_{L^2(\Omega)} + \|u(x,0)\|_{H^1(\Omega)}) + Ch(\|\partial_t g\|_{L^\infty(0,T,L^2(\Omega))} \\ &\quad + \|\partial_t^2 g\|_{L^2(\Omega_T)} + \|\partial_t^2 u(x,0)\|_{H^1(\Omega)} + \|\partial_t^3 u(x,0)\|_{L^2(\Omega)}). \end{aligned} \tag{2.20}$$

The constant C depends on $a_{\min}$, $a_{\max}$, $K_{\min}$, $K_{\max}$, *and T.*

The following Theorem 2.4 gives us the error estimate for the scheme (2.18).

Theorem 2.4. *Suppose that Cordes Condition 2.1 and Assumption 2.2 hold, we have*

$$\begin{aligned}\|(\partial_t u_h-\partial_t v_h)(\cdot,T)\|_{L^2(\Omega)}+\|(u_h-v_h)(\cdot,T)\|_{H^1(\Omega)}\\ \leqslant C\Delta t(1+h^{-1})(\|\partial_t g\|_{L^\infty(0,T,L^2(\Omega))}+\|\partial_t^2 g\|_{L^2(\Omega_T)}\\ +\|\partial_t^2 u(x,0)\|_{H^1(\Omega)}+\|\partial_t^3 u(x,0)\|_{L^2(\Omega)}).\end{aligned}\tag{2.21}$$

The constant C depends on C_X, *T*, $a_{\min}$, $a_{\max}$, $K_{\min}$, $K_{\max}$, μ_σ, *and* $\|(\mathrm{Trace}[\sigma])^{-1}\|_{L^\infty(\Omega)}$.

3. Proofs

The proofs are organized into three subsections corresponding to the three subsections of Section 2.

3.1. Compensation phenomena: proof of Theorem 2.1

Lemma 3.1. *We have*

$$\|\partial_t^2 u\|^2_{L^2(\Omega)}(T)+a[\partial_t u](T)\leqslant C\left(T,\frac{K_{\max}}{K_{\min}},K_{\max}\right)\times\left(a[\partial_t u](0)+\|\partial_t^2 u(x,0)\|^2_{L^2(\Omega)}+\|\partial_t g\|^2_{L^2(\Omega_T)}\right).\tag{3.1}$$

Proof. In case a is smooth, differentiating (1.1) with respect to t, we have

$$K^{-1}\partial_t^3 u-\mathrm{w}a\nabla\partial_t u=\partial_t g.\tag{3.2}$$

multiplying by $\partial_t^2 u$, and integrating over Ω, we obtain that

$$\frac{1}{2}\frac{\mathrm{d}}{\mathrm{d}t}\left\|K^{-\frac{1}{2}}\partial_t^2 u\right\|^2_{L^2(\Omega)}+\frac{1}{2}\frac{\mathrm{d}}{\mathrm{d}t}a[\partial_t u]=(\partial_t g,\partial_t^2 u)_{L^2(\Omega)}.\tag{3.3}$$

Integrating the latter equation with respect to t and using Cauchy–Schwartz inequality we obtain that

$$\left\|K^{-\frac{1}{2}}\partial_t^2 u\right\|^2_{L^2(\Omega)}(T)+a[\partial_t u](T)\leqslant\left\|K^{-\frac{1}{2}}\partial_t^2 u\right\|^2_{L^2(\Omega)}(0)+a[\partial_t u](0)+\|\partial_t g\|_{L^2(\Omega_T)}\|\partial_t^2 u\|_{L^2(\Omega_T)}.\tag{3.4}$$

Consider the following differential inequality, suppose that A is constant, $B(t)>0$ and non-decrease, $X(t)>0$ and $X(t)$ is continuous with respect to t

$$X(t)\leqslant A+B(t)\left(\int_0^t X(s)\mathrm{d}s\right)^{\frac{1}{2}}.\tag{3.5}$$

Write $Y(t)=\sup_{s\in[0,t]}X(s)$, one has

$$X(t)\leqslant A+B(t)t^{\frac{1}{2}}(Y(t))^{\frac{1}{2}}\leqslant A+\frac{t(B(t))^2+Y(t)}{2}.\tag{3.6}$$

Take the supremum of both sides over $t\in[0,T]$, we have

$$Y(T)\leqslant 2A+T(B(T))^2.\tag{3.7}$$

It follows that

$$\|\partial_t^2 u\|^2_{L^2(\Omega)}(T)+a[\partial_t u](T)\leqslant C\left(T,\frac{K_{\max}}{K_{\min}},K_{\max}\right)(a[\partial_t u](0)+\|\partial_t^2 u\|^2_{L^2(\Omega)}(0)+\|\partial_t g\|^2_{L^2(\Omega_T)}).\tag{3.8}$$

In the case where a is non-smooth we use Galerkin approximations of u in (1.1) and then pass to limit. This technique is standard and we refer to [14, Section 7.3.2.c] for a reminder. □

Lemma 3.2

$$\|\partial_t u\|^2_{L^2(\Omega)}(T)+a[u](T)\leqslant C\left(T,\frac{K_{\max}}{K_{\min}},K_{\max}\right)(a[u](0)+\|\partial_t u\|^2_{L^2(\Omega)}(0)+\|g\|^2_{L^2(\Omega_T)}).\tag{3.9}$$

Proof. Multiplying (1.1) by $\partial_t u$, and integrating over Ω, we obtain that

$$\frac{1}{2}\frac{\mathrm{d}}{\mathrm{d}t}\left\|K^{-\frac{1}{2}}\partial_t u\right\|^2_{L^2(\Omega)}+\frac{1}{2}\frac{\mathrm{d}}{\mathrm{d}t}a[u]=(g,\partial_t u)_{L^2(\Omega)}.\tag{3.10}$$

The remaining part of the proof is similar to the proof of Lemma 3.1. □

We now need a variation of Campanato's result [12] on non-divergence form elliptic operators. For a symmetric matrix M, let us write

$$\nu_M:=\frac{\mathrm{Trace}(M)}{\mathrm{Trace}({}^tMM)}.\tag{3.11}$$

Consider the following Dirichlet problem:

$$L_M v=f\tag{3.12}$$

with $L_M:=\sum_{i,j=1}^2 M_{ij}(x)\partial_i\partial_j$ and homogeneous Dirichlet boundary condition. The following Theorem 3.1 is an adaptation of Theorem 1.2.1 of [25]. They are proved in [25] under the assumption that M is bounded and elliptic. It can be proved that the conditions $\mu_M<\infty$ and $\nu_M<\infty$ are sufficient for the validity of the theorem, we refer to [28,29] for that proof.

Theorem 3.1. *Assume that* $\mu_M<\infty$, $\nu_M\in L^\infty(\Omega)$ *and* Ω *is convex. If* $f\in L^2(\Omega)$ *the Dirichlet problem (3.12) has a unique solution satisfying*

$$\|v\|_{H^2(\Omega)}\leqslant C\mu_M\|\nu_M f\|_{L^2(\Omega)}.\tag{3.13}$$

Remark 3.1. The theorem can be extended to dimension $n>2$ under the general Cordes condition [25].

Let us now prove the compensation result in Theorem 2.1. Choose

$$M:=\frac{\sigma}{|\det(\nabla F)|^{\frac{1}{2}}}\circ F^{-1}.\tag{3.14}$$

Recall that $\sigma:={}^t\nabla F a\nabla F$. (3.14) is well defined since $\mu_M=\mu_\sigma$ and

$$\|\nu_M\|^2_{L^\infty(\Omega)}\leqslant\frac{C}{\lambda_{\min}(a)}\|(\mathrm{Trace}[\sigma])^{-1}\|^2_{L^\infty(\Omega)}.\tag{3.15}$$

Fix $t\in[0,T]$. Choose

$$f:=\frac{(K^{-1}\partial_t^2 u-g)}{|\det(\nabla F)|^{\frac{1}{2}}}\circ F^{-1}.\tag{3.16}$$

By the change of variable $y=F(x)$, one obtains that

$$\|f\|_{L^2(\Omega)}\leqslant 2K^{-1}_{\min}\|\partial_t^2 u\|_{L^2(\Omega)}+2\|g\|_{L^2(\Omega)}.\tag{3.17}$$

Using the notation $\tilde{K}(y):=K(F^{-1}(y))$, $\tilde{g}(y,t):=g(F^{-1}(y),t)$, and $\tilde{u}(y,t):=u(F^{-1}(y),t)$, it follows from Theorem 3.1 that there exists a unique $v\in H^2(\Omega)$ such that

$$\sum_{i,j}(\sigma(F^{-1}(y)))_{i,j}\partial_i\partial_j v(y,t)=\tilde{K}^{-1}(y)\partial_t^2\tilde{u}(y,t)-\tilde{g}(y,t)\tag{3.18}$$

and

$$\|v\|_{H^2(\Omega)}\leqslant C\mu_M\|\nu_M\|_{L^\infty(\Omega)}(K^{-1}_{\min}\|\partial_t^2 u\|_{L^2(\Omega)}+\|g\|_{L^2(\Omega)}).\tag{3.19}$$

By $y=F(x)$ and the identity $\mathrm{div}\,a\nabla F=0$ we deduce that (3.18) can be written as

$$\mathrm{div}\,(a\nabla(v\circ F))=K^{-1}\partial_t^2 u-g.\tag{3.20}$$

If $\partial_t^2 u \in L^2(\Omega)$ and $g(\cdot,t) \in L^2(\Omega)$ we can use the uniqueness property for the solution of the following divergence form elliptic equation (with homogeneous Dirichlet boundary condition):

$$\operatorname{div}(a\nabla u) = K^{-1}\partial_t^2 u - g \tag{3.21}$$

to obtain that $v \circ F = u$. Thus, we have proven Theorem 2.1.

3.2. Numerical homogenization in space: proof of Theorem 2.2

In the following sections we will prove the convergence of semidiscrete and fully discrete numerical homogenization formulation (2.14) and (2.18).

We have the following lemmas which are the discrete analogs of Lemmas 3.1 and 3.4.

Lemma 3.3. *We have*

$$\|\partial_t^2 u_h\|^2_{L^2(\Omega)}(T) + a[\partial_t u_h](T) \leqslant C\left(T, \frac{K_{\max}}{K_{\min}}, K_{\max}\right)(a[\partial_t u_h](0) + \|\partial_t^2 u_h(x,0)\|^2_{L^2(\Omega)} + \|\partial_t g\|^2_{L^2(\Omega_T)}). \tag{3.22}$$

Lemma 3.4

$$\|\partial_t u_h\|^2_{L^2(\Omega)}(T) + a[u_h](T) \leqslant C\left(T, \frac{K_{\max}}{K_{\min}}, K_{\max}\right)(a[u_h](0) + \|\partial_t u_h\|^2_{L^2(\Omega)}(0) + \|g\|^2_{L^2(\Omega)_T}). \tag{3.23}$$

Write $\mathscr{R}_h$ the projection operator mapping $L^2(0,T;H^1_0(\Omega))$ onto Y^h_T, such that for all $v \in Y^h_T$:

$$\mathscr{A}_T[v, u - \mathscr{R}_h u] = 0 \tag{3.24}$$

let $\rho := u - \mathscr{R}_h u$ and $\theta := \mathscr{R}_h u - u_h$, where u_h is the solution of (2.14).

For fixed $t \in [0,T]$ and $v \in H^1_0(\Omega)$, we write $\mathscr{R}_{h,t}v(\cdot,t)$ the solution of

$$\int_\Omega {}^t\nabla\psi a(x)\nabla(v - \mathscr{R}_{h,t}v(x,t))\mathrm{d}x = 0 \quad \text{for all } \psi \in V^h. \tag{3.25}$$

It is obvious that $\mathscr{R}_h u(\cdot,t) = \mathscr{R}_{h,t}u(\cdot,t)$. For example, we can choose a series of test functions in (3.24) which is separable in space and time, $v(x,t) = T(t)X(x)$, $T(t)$ is smooth in t and has $\delta(t)$ function as its weak limit.

We need the following lemma:

Lemma 3.5. *For $v \in H^1_0(\Omega)$ we have*

$$(a[v - \mathscr{R}_{h,t}v])^{\frac12} \leqslant Cha^{\frac12}_{\max}\mu_\sigma^{\frac14}\|\tilde v\|_{H^2(\Omega)}. \tag{3.26}$$

Proof. Using the change of coordinates $y = F(x)$ we obtain that (write $\tilde v := v \circ F^{-1}$)

$$a[v] = Q[\tilde v] \tag{3.27}$$

with

$$\mathscr{Q}[w] := \int_\Omega {}^t\nabla w(y)Q(y)\nabla w(y)\mathrm{d}y \tag{3.28}$$

and

$$Q(y) := \frac{\sigma}{\det(\nabla F)} \circ F^{-1}. \tag{3.29}$$

Using the definition of $\mathscr{R}_h v$ we derive that

$$\mathscr{Q}[\tilde v - \mathscr{R}_h v \circ F^{-1}] = \inf_{\varphi \in X^h} \mathscr{Q}[\tilde v - \varphi]. \tag{3.30}$$

By interpolation property (2.7) it follows,

$$\mathscr{Q}[\tilde v - \mathscr{R}_h v \circ F^{-1}] \leqslant \lambda_{\max}(Q)C_X^2 h^2\|\tilde v\|^2_{H^2(\Omega)}, \tag{3.31}$$

where $\lambda_{\max}(Q)$ is the supremum of eigenvalues of Q over Ω.

It is easy to obtain that

$$\lambda_{\max}(Q) \leqslant Ca_{\max}\mu_\sigma^{\frac12} \tag{3.32}$$

which finishes the proof. □

We will use Lemmas 3.5–3.9 to obtain the approximation property of the projection operator $\mathscr{R}_h$.

With the improved Assumption 2.2, differentiate (1.1) with respect to t, and follow the proof of Theorem 2.1, we have

Lemma 3.6. *$\partial_t(u \circ F^{-1}) \in L^\infty(0,T,H^2(\Omega))$ and*

$$\|\partial_t(u \circ F^{-1})\|_{L^\infty(0,T,H^2(\Omega))} \leqslant C(\|\partial_t g\|_{L^\infty(0,T,L^2(\Omega))} + \|\partial_t^2 g\|_{L^2(\Omega_T)} + \|\partial_t^3 u(x,0)\|_{L^2(\Omega)} + \|\partial_t^2 u(x,0)\|_{H^1(\Omega)}). \tag{3.33}$$

The constant C is the one given in Theorem 2.1.

Apply Lemma 3.5 to $\partial_t u$, we have

Lemma 3.7

$$(\mathscr{A}_T[\partial_t\rho])^{\frac12} \leqslant Ch(\|\partial_t g\|_{L^\infty(0,T,L^2(\Omega))} + \|\partial_t^2 g\|_{L^2(\Omega_T)} + \|\partial_t^3 u(x,0)\|_{L^2(\Omega)} + \|\partial_t^2 u(x,0)\|_{H^1(\Omega)}). \tag{3.34}$$

The constant C depends on C_X, n, Ω, μ_σ, $a_{\min}$, $a_{\max}$, $K_{\min}$,$K_{\max}$, and $\|(\mathrm{Trace}[\sigma])^{-1}\|_{L^\infty(\Omega)}$.

We have the following estimate for $\|\partial_t\rho\|$ using the so-called Aubin–Nitsche trick [5].

Lemma 3.8

$$\|\partial_t\rho\|_{L^2(\Omega_T)} \leqslant Ch^2(\|\partial_t g\|_{L^\infty(0,T,L^2(\Omega))} + \|\partial_t^2 g\|_{L^2(\Omega_T)} + \|\partial_t^3 u(x,0)\|_{L^2(\Omega)} + \|\partial_t^2 u(x,0)\|_{H^1(\Omega)}). \tag{3.35}$$

The constant C in Lemma depends on C_X, n, Ω, μ_σ, $a_{\min}$, $a_{\max}$, $K_{\min}$, $K_{\max}$, and $\|(\mathrm{Trace}[\sigma])^{-1}\|_{L^\infty(\Omega)}$

Proof. We choose $v \in L^2(0,T,H^1_0(\Omega))$ to be the solution of the following linear problem: for all $w \in L^2(0,T,H^1_0(\Omega))$

$$A_T[w,v] = (w, \partial_t\rho)_{L^2(\Omega_T)}. \tag{3.36}$$

Choosing $w = \partial_t\rho$ in Eq. (3.36) we deduce that

$$\|\partial_t\rho\|^2_{L^2(\Omega_T))} = \mathscr{A}_T[\partial_t\rho, v - \mathscr{R}_h v]. \tag{3.37}$$

Using Cauchy–Schwartz inequality we deduce that

$$\|\partial_t\rho\|^2_{L^2(\Omega_T)} \leqslant (\mathscr{A}_T[\partial_t\rho])^{\frac12}(\mathscr{A}_T[v - \mathscr{R}_h v])^{\frac12}. \tag{3.38}$$

Since $\partial_t\rho(\cdot,t) \in L^2(\Omega)$, applying Theorem 3.1 for $t \in [0,T]$ then integrate over t, we obtain that

$$\|\hat v\|_{L^2(0,T,H^2(\Omega))} \leqslant C\|\partial\rho\|_{L^2(\Omega_T)}. \tag{3.39}$$

Using Lemma 3.5 we obtain that

$$(\mathscr{A}_T[v - \mathscr{R}_h v])^{\frac12} \leqslant Ch\|\partial_t\rho\|_{L^2(\Omega_T)}. \tag{3.40}$$

It follows that

$$\|\partial_t\rho\|_{L^2(\Omega_T)} \leqslant Ch(\mathscr{A}_T[\partial_t\rho])^{\frac12}. \tag{3.41}$$

We deduce the lemma by applying Lemma 3.8 to bound $A_T[\partial_t\rho]$. □

We have the following estimates for initial data.

Lemma 3.9.

$$\|\mathscr{R}_{h,0}\partial_t u(x,0)-\partial_t u(x,0)\|_{L^2(\Omega)}\leqslant Ch^2(\|\partial_t g(x,0)\|_{L^2(\Omega)}+\|\partial_t^2 u(x,0)\|_{H^1(\Omega)}+\|\partial_t^3 u(x,0)\|_{L^2(\Omega)})$$
$$\|\mathscr{R}_{h,0}u(x,0)-u(x,0)\|_{H^1_0(\Omega)}\leqslant Ch(\|\partial_t g(x,0)\|_{L^2(\Omega)}+\|\partial_t^2 u(x,0)\|_{H^1(\Omega)}+\|\partial_t^3 u(x,0)\|_{L^2(\Omega)}) \quad (3.42)$$

Proof. We can estimate $\|\partial_t\rho\|_{L^2(\Omega)}$ using the duality argument similar to Lemma 3.8 and derive the second inequality by Lemma 3.5. □

Lemma 3.10. *we have*

$$\|\partial_t(u-u_h)\|^2_{L^2(\Omega)}(T)+a[u-u_h](T)\leqslant C(K_{\min},K_{\max},T)(\|\partial_t(u-u_h)\|^2_{L^2(\Omega)}(0)+a[u-u_h](0)+\|\partial_t\rho\|_{L^2(\Omega_T)}\|\partial_t^2(u-u_h)\|_{L^2(\Omega_T)}+\mathscr{A}_T[\partial_t\rho]). \quad (3.43)$$

Proof. For $\psi\in L^2(0,T,H^1_0(\Omega))$, we have

$$(K^{-1}\psi,\partial_t^2(u-u_h))+a[\psi,u-u_h]=0. \quad (3.44)$$

Let $\psi=\partial_t\theta=\partial_t(u-u_h)-\partial_t\rho$, it follows

$$\frac{1}{2}\frac{\mathrm{d}}{\mathrm{d}t}\left\|K^{-\frac{1}{2}}\partial_t(u-u_h)\right\|^2_{L^2(\Omega)}+\frac{1}{2}\frac{\mathrm{d}}{\mathrm{d}t}a[u-u_h]=(K^{-1}\partial_t\rho,\partial_t^2(u-u_h))+a[\partial_t\rho,u-u_h]. \quad (3.45)$$

Integrate with respect to t, using Cauchy–Schwartz inequality, we have

$$\frac{1}{2}\left\|K^{-\frac{1}{2}}\partial_t(u-u_h)\right\|^2_{L^2(\Omega)}(T)-\frac{1}{2}\left\|K^{-\frac{1}{2}}\partial_t(u-u_h)\right\|^2_{L^2(\Omega)}(0)+\frac{1}{2}a[u-u_h](T)-\frac{1}{2}a[u-u_h](0)\leqslant\int_0^T K^{-1}_{\min}\|\partial_t\rho\|_{L^2(\Omega)}\|\partial_t^2(u-u_h)\|_{L^2(\Omega)}\mathrm{d}t+(\mathscr{A}_T[\partial_t\rho]\mathscr{A}_T[u-u_h])^{\frac{1}{2}}. \quad (3.46)$$

The remaining part of the proof is similar to Lemma 3.1. □

Theorem 2.2 is a straightforward combination of Lemmas 3.1, 3.3, 3.7–3.10.

3.3. Numerical homogenization in space and time: proof of Theorems 2.3 and 2.4

3.3.1. Stability

Choose $\psi\in U^h_T$ in Eq. (2.18) such that $\psi(x,t)=\partial_t v_h(x,t)$ for $t\in(t_n,t_{n+1}]$. We obtain that

$$\left\|K^{-\frac{1}{2}}\partial_t v_h\right\|^2_{L^2(\Omega)}(t_{n+1})-(K^{-1}\partial_t v_h(t_{n+1}),\partial_t v_h(t_n))_{L^2(\Omega)}=-\int_{t_n}^{t_{n+1}}a[\partial_t v_h,v_h]\mathrm{d}t+\int_{t_n}^{t_{n+1}}(\partial_t v_h,g)_{L^2(\Omega)}\mathrm{d}t. \quad (3.47)$$

Observing that

$$\int_{t_n}^{t_{n+1}}a[\partial_t v_h,v_h]\mathrm{d}t=\frac{1}{2}a[v_h](t_{n+1})-\frac{1}{2}a[v_h](t_n). \quad (3.48)$$

using Cauchy–Schwartz inequality it follows:

$$\|K^{-\frac{1}{2}}\partial_t v_h\|^2(t_{n+1})+a[v_h](t_{n+1})\leqslant\|K^{-\frac{1}{2}}\partial_t v_h\|^2(t_n)+a[v_h](t_n)+2\int_{t_n}^{t_{n+1}}(\partial_t v_h,g)_{L^2(\Omega)}(t)\,\mathrm{d}t. \quad (3.49)$$

Summing over n from 0 to $M-1$, we have

$$\|K^{-\frac{1}{2}}\partial_t v_h\|^2(T)+a[v_h](T)\leqslant\|K^{-\frac{1}{2}}\partial_t v_h\|^2(0)+a[v_h](0)+2\times\int_0^T(\partial_t v_h,g)_{L^2(\Omega)}\,\mathrm{d}t. \quad (3.50)$$

We conclude the proof of Theorem 2.3 using the inequality (3.7) in the proof of Lemma 3.1.

3.3.2. H^1 error estimate

We derive from Eqs. (2.18) and (2.14) that

$$(K^{-1}\psi,\partial_t u_h-\partial_t v_h)(t_{n+1})-(K^{-1}\psi,\partial_t u_h-\partial_t v_h)(t_n)-\int_{t_n}^{t_{n+1}}(K^{-1}\partial_t\psi,\partial_t u_h-\partial_t v_h)\mathrm{d}t+\int_{t_n}^{t_{n+1}}a[\psi,u_h-v_h]\mathrm{d}t=0. \quad (3.51)$$

Let $\psi=\partial_t\hat{u}_h-\partial_t v_h$ where $\hat{u}_h$ is the linear interpolation of u_h over Z^h_T. Write $y_h=u_h-v_h$ and $w_h=\hat{u}_h-u_h$, it follows that

$$(K^{-1}\partial_t y_h,\partial_t y_h)(t_{n+1})+(K^{-1}\partial_t w_h,\partial_t y_h)(t_{n+1})-(K^{-1}\partial_t y_h,\partial_t y_h)(t_n)-(K^{-1}\partial_t w_h,\partial_t y_h)(t_n)+\int_{t_n}^{t_{n+1}}a[\partial_t y_h,y_h]\mathrm{d}t+\int_{t_n}^{t_{n+1}}a[\partial_t w_h,y_h]\mathrm{d}t=0. \quad (3.52)$$

Observing $\int_{t_n}^{t_{n+1}}\partial_t w_h(x,t)\,dt=0$ we need the following lemma, which is a slight variation of the Hilbert–Bramble lemma, [11]

Lemma 3.11. *If* $\int_{t_n}^{t_{n+1}}u(s)\mathrm{d}s=0$, *then*

$$u^2\leqslant\frac{1}{4}\Delta t\int_{t_n}^{t_{n+1}}u'(s)^2\,\mathrm{d}s. \quad (3.53)$$

Since $\partial_t^2 w_h(x,t)=-\partial_t^2 u_h(x,t)$ in $(t_n,t_{n+1}]$, by Lemma 3.11 we have

$$\int_\Omega|\partial_t w_h(x,t)|^2\mathrm{d}x\,\mathrm{d}t\leqslant\frac{1}{4}\Delta t\int_{t_n}^{t_{n+1}}\int_\Omega|\partial_t^2 u_h(x,t)|^2\,\mathrm{d}x\,\mathrm{d}t, \quad (3.54)$$

and

$$\int_{t_n}^{t_{n+1}}\int_\Omega|\partial_t w_h(x,t)|^2\,\mathrm{d}x\,\mathrm{d}t\leqslant\frac{1}{4}\Delta t^2\int_{t_n}^{t_{n+1}}\int_\Omega|\partial_t^2 u_h(x,t)|^2\,\mathrm{d}x\,\mathrm{d}t. \quad (3.55)$$

Using the inverse Sobolev inequality (2.9) we obtain from Eq. (3.55) that

$$\int_{t_n}^{t_{n+1}}\int_\Omega a[\partial_t w_h]\,\mathrm{d}x\,\mathrm{d}t\leqslant C\frac{\Delta t^2}{h^2}\int_{t_n}^{t_{n+1}}\int_\Omega|\partial_t^2 u_h(x,t)|^2\,\mathrm{d}x\,\mathrm{d}t. \quad (3.56)$$

Summing (3.52) over n, notice $y_h(0)=0$, $\partial_t y_h(0)=0$ we obtain that

$$(K^{-1}\partial_t y_h,\partial_t y_h)_{L^2(\Omega)}(T)+\frac{1}{2}a[y_h(\cdot,T)]=-\int_0^T a[\partial_t w_h,y_h]\mathrm{d}t-(K^{-1}\partial_t w_h,\partial_t y_h)_{L^2(\Omega)}(T). \quad (3.57)$$

Theorem 2.4 is a straightforward consequence of (3.57), the estimates (3.54), (3.56), Lemmas 3.3 and 3.9.

4. Numerical experiments

In this section, we will present the numerical algorithm and examples.

We use web extended B-spline based finite element [19] to span the space X^h introduced in Section 2.2. For all the numerical examples, we compute the solutions up to time $T=1$. The initial condition is $u(x,0)=0$ and $u_t(x,0)=0$. The boundary condition is $u(x,t)=0$, $x\in\partial\Omega$. For simplicity, the computational domain is the square $[-1,1]\times[-1,1]$ in dimension two.

We have a fine mesh and a coarse mesh characterized by different degrees of freedom (*dof*). In general, the fine mesh is generated by hierarchical refinement of the coarse mesh: for each triangle of the coarse mesh, choose middle points of its 3 edges as new vertices, and divide the triangle into 4 new triangles. a is defined as a piecewise constant function over each fine mesh triangle, and is evaluated at the center of mass of the triangle.

Algorithm 4.1. Algorithm for numerical homogenization

1. Compute F on fine mesh, the fine mesh solver for F is *Matlab* routine *assempde*.
2. Construct multi-scale finite element basis $\psi = \varphi \circ F$, compute stiffness matrix K and mass matrix M.
3. March (2.18) and (2.19) in time with respect to the coarse *dof*.
4. Repeat 3 if we have multiple right hand sides.

In the implementation, F is approximated by a piecewise linear finite element solution. We mesh the square such that no triangle has an obtuse angle, therefore F is an invertible piecewise linear mapping [17]. When we construct ψ, we simply take its piecewise linear interpolation on the fine mesh.

All the computations were done at a single Opteron Dual-Core 2600 cpu of a Sun Fire X4600 server, and programmed in Matlab 7.3.

Example 4.1. Multi-scale trigonometric coefficients

The following example is extracted from [26] as a problem without scale separation:

$$a(x) = \frac{1}{6}\left(\frac{1.1+\sin(2\pi x/\epsilon_1)}{1.1+\sin(2\pi y/\epsilon_1)} + \frac{1.1+\sin(2\pi y/\epsilon_2)}{1.1+\cos(2\pi x/\epsilon_2)} + \frac{1.1+\cos(2\pi x/\epsilon_3)}{1.1+\sin(2\pi y/\epsilon_3)} + \frac{1.1+\sin(2\pi y/\epsilon_4)}{1.1+\cos(2\pi x/\epsilon_4)} + \frac{1.1+\cos(2\pi x/\epsilon_5)}{1.1+\sin(2\pi y/\epsilon_5)} + \sin(4x^2y^2)+1\right), \tag{4.1}$$

where $\epsilon_1 = \frac{1}{5}$, $\epsilon_2 = \frac{1}{13}$, $\epsilon_3 = \frac{1}{17}$, $\epsilon_4 = \frac{1}{31}$, $\epsilon_5 = \frac{1}{65}$. The conductivity a is smooth, therefore it satisfies Cordes Condition 2.1.

First, we want to compare the performance of different numerical homogenization methods

- LFEM: A multi-scale finite element where F is computed locally (instead of globally) on each triangle K of the coarse mesh as the solution of a cell problem with boundary condition $F(x) = x$ on ∂K. This method has been implemented in order to understand the effect of the removal of global information in the structure of the metric induced by F.
- FEM_ψ_{lin}: The Galerkin scheme using the finite elements $\psi_i = \varphi_i \circ F$, where φ_i are the piecewise linear nodal basis elements.
- FEM_ψ_{sp}: The Galerkin scheme using the finite element $\psi_i = \varphi_i \circ F$, where φ_i are weighted cubic B-spline elements.

Suppose u_f is the finite element solution of (1.1) computed on the fine mesh at time $T = 1$, the fine mesh solver is *Matlab* routine *hyperbolic*, which uses linear finite element basis in space and adaptive ODE integrator in time. v_h is the solution of (2.18). Numerical errors in the norm $\|\cdot\|$ are computed by

$$\text{error} = \frac{\|v_h - u_f\|}{\|u_f\|}. \tag{4.2}$$

Numerical errors in L^1, L^2, L^∞ and H^1 norm are computed.

In Table 1 performances of different methods with coarse mesh *dof* 49 are compared. We observe that the methods using global F have better performance, and FEM_ψ_{sp} is much better than other methods. Note that the improvement of FEM_ψ_{lin} over LFEM is not as significant as the elliptic case [29].

From now on, all the results are computed by the method FEM_ψ_{sp}.

Next, the impact of right hand side on accuracy will be investigated. We solve Eq. (1.1) with a time independent source term $g = 1$, a slowly varying term $g = \sin(2.4x - 1.8y + 2\pi t)$, and a Gaussian source term given by

$$g(x,y) = \frac{1}{\sqrt{2\pi\sigma^2}} \exp\left(-\frac{x^2 + (y-0.15)^2}{2\sigma^2}\right), \tag{4.3}$$

with $\sigma = 0.05$. Notice that as $\sigma \to 0$, the source function will become singular in space.

Table 2 presents the errors for time independent term $g = 1$. Table 3 presents the errors for slowly varying source term $g = \sin(2.4x - 1.8y + 2\pi t)$. Table 4 presents the errors for relatively singular Gaussian forcing term. It is clear that if the source term is time independent and smooth in space, the method is more accurate, which corresponds to the smoothness requirement of g in Theorem 2.4. In all the examples, we have tried two fine meshes which have *dof* 65,025 and 261,121, respectively, roughly

Table 1
Example 4.1, numerical errors of different methods, coarse *dof* 49, fine *dof* 261,121, $g = 1$

Method	L^1	L^∞	L^2	H^1
LFEM	0.0440	0.0982	0.0534	0.2054
FEM_ψ_{lin}	0.0315	0.0518	0.0362	0.1601
FEM_ψ_{sp}	0.0021	0.0035	0.0022	0.0189

Table 2
Example 4.1, numerical errors of FEM_ψ_{sp}, with $g = 1$, dof_f is fine mesh *dof*, dof_c is coarse mesh *dof*

dof_f	dof_c	L^1	L^∞	L^2	H^1
65,025	9	0.0075	0.0118	0.0074	0.0394
	49	0.0023	0.0037	0.0023	0.0194
	225	0.0009	0.0023	0.0010	0.0117
261,121	9	0.0070	0.0106	0.0069	0.0373
	49	0.0021	0.0035	0.0022	0.0188
	225	0.0009	0.0025	0.0010	0.0117

Table 3
Example 4.1, numerical errors of FEM_ψ_{sp}, with $g = \sin(2.4x - 1.8y + 2\pi t)$

dof_f	dof_c	L^1	L^∞	L^2	H^1
65,025	9	0.0400	0.0390	0.0360	0.0869
	49	0.0107	0.0105	0.0096	0.0393
	225	0.0035	0.0047	0.0033	0.0233
261,121	9	0.0399	0.0373	0.0359	0.0866
	49	0.0104	0.0109	0.0095	0.0391
	225	0.0034	0.0047	0.0033	0.0231

Table 4
Example 4.1, numerical errors of FEM_ψ_{sp}, with the Gaussian source g in (4.3)

dof_f	dof_c	L^1	L^∞	L^2	H^1
65,025	9	0.0581	0.2270	0.0704	0.3484
	49	0.0272	0.1023	0.0333	0.2305
	225	0.0096	0.0179	0.0095	0.0957
261,121	9	0.0574	0.2199	0.0688	0.3436
	49	0.0274	0.976	0.0332	0.2254
	225	0.0097	0.0212	0.0101	0.1005

250×250 and 500×500. It can be seen that for fixed coarse *dof*, the errors with respect to different fine *dof* are pretty close, which means fine *dof* 65,025 is enough for this problem.

The Fig. 1 shows the L^1 error evolution with respect to time, which is typical for all norms. The overshoot at the beginning is proportional to the time discretization step. After several steps, the errors tend to be stable.

Example 4.2. Time independent high conductivity channel

High conductivity channel is an interesting test problem in many petroleum applications because of its strong non-local effects. In this example, a is characterized by a narrow and long range high conductivity channel. We choose $a(x) = A \gg 1$, if x is in the channel, and $a(x) = 1$, if x is not in the channel. The media is illustrated in Fig. 2. However, in this case, whether or not Cordes Condition 2.1 is not clear. We will go ahead testing the numerical performance of our method.

Table 5 shows numerical errors for $g = 1$ with fixed coarse *dof* 49 and $A = 10^1, 10^2, 10^3, 10^4$, respectively. From the table we can see that the errors grow with the aspect ratio increasing, but the growth is moderate and the numerical behavior of the method is stable. The errors for time dependent right hand side $g = \sin(2.4x - 1.8y + 2\pi t)$ with $A = 10^2$ are also given in Table 6.

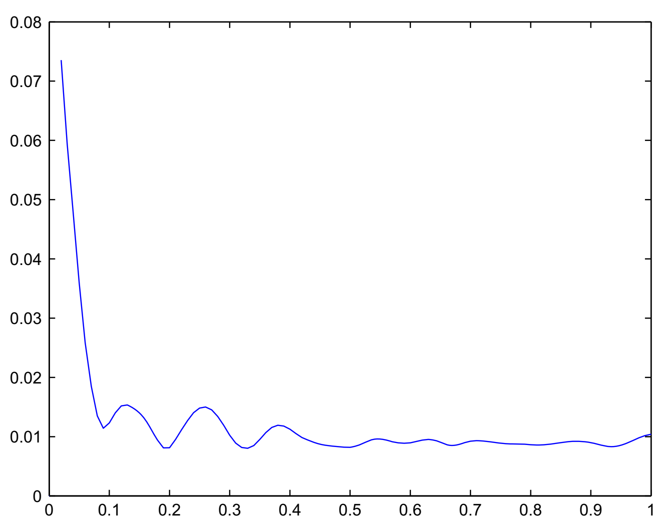

Fig. 1. Example 4.1, L^1 error with respect to time, for $g = 1$, coarse *dof* 9, fine *dof* 65025.

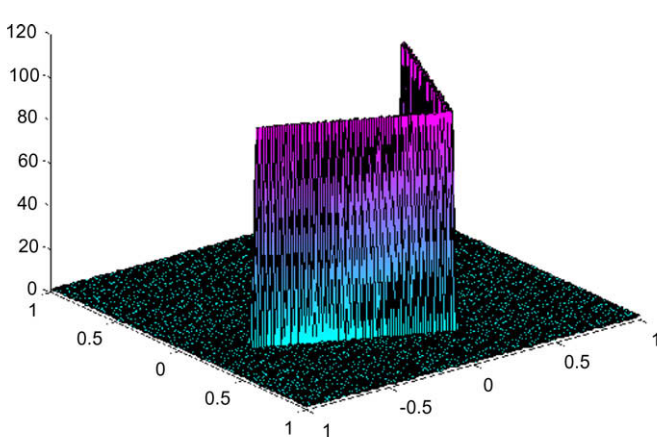

Fig. 2. Example 4.2, high conductivity channel medium.

Table 5
Example 4.2, numerical errors with respect to different aspect ratios, coarse *dof* 49, fine *dof* 261121

A	L^1	L^∞	L^2	H^1
10	0.0021	0.0056	0.0025	0.0240
100	0.0118	0.0497	0.0180	0.0964
1000	0.0181	0.0931	0.0316	0.1308
10,000	0.0243	0.1174	0.0419	0.1550

Table 6
Example 4.2, numerical errors for $g = \sin(2.4x - 1.8y + 2\pi t)$

dof_f	dof_c	L^1	L^∞	L^2	H^1
65,025	9	0.0750	0.0777	0.0729	0.1528
	49	0.0301	0.0351	0.00298	0.0779
	225	0.0096	0.0118	0.0092	0.0324
261,121	9	0.0752	0.0779	0.0731	0.1533
	49	0.0302	0.0345	0.0299	0.0782
	225	0.0094	0.0116	0.0091	0.0321

Example 4.3. Time independent site percolation

In this example, we consider the site percolating medium associated to Fig. 3. In this case, we subdivide the square into a 64×64 checkerboard, the conductivity of each site is equal to γ or $1/\gamma$ with probability 1/2. We have chosen $\gamma = 10$ in this example. In fact, this medium may not satisfy the Cordes Condition 2.1 (also refer to Remark 2.1). However, we will show that the method still works fine for this example.

Fig. 4 shows u computed with 261121 *dof* and v_h computed with 9 *dof* in the case $g = 1$ at time 1 using method FEM_ψ_{sp}. They are visually almost the same even for small scale features. Table 7 gives the numerical errors for $g = 1$ with respect to different coarse and fine *dof*.

Finally, we consider the site percolating medium, with Neumann boundary condition and a more realistic forcing term. The source term is given by $g(x,t) = T(t)X(x,y)$, $X(x,y)$ is the Gaussian source function described by

$$X(x,y) = \frac{1}{\sqrt{2\pi\sigma^2}} \exp\left(-\frac{x^2+y^2}{2\sigma^2}\right), \tag{4.4}$$

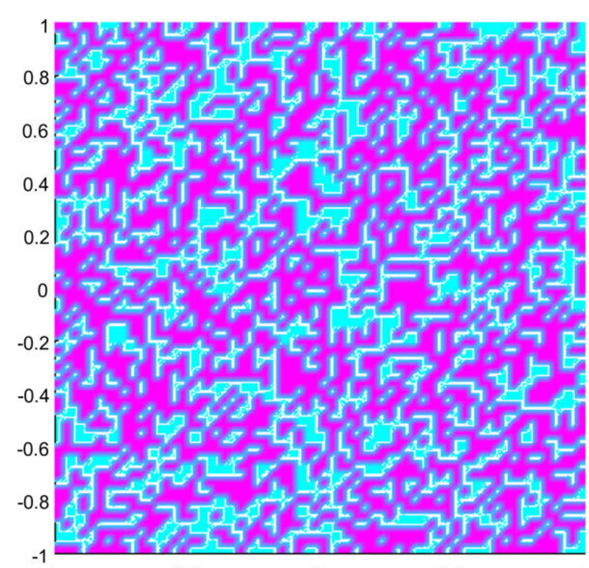

Fig. 3. Example 4.3, site percolation medium.

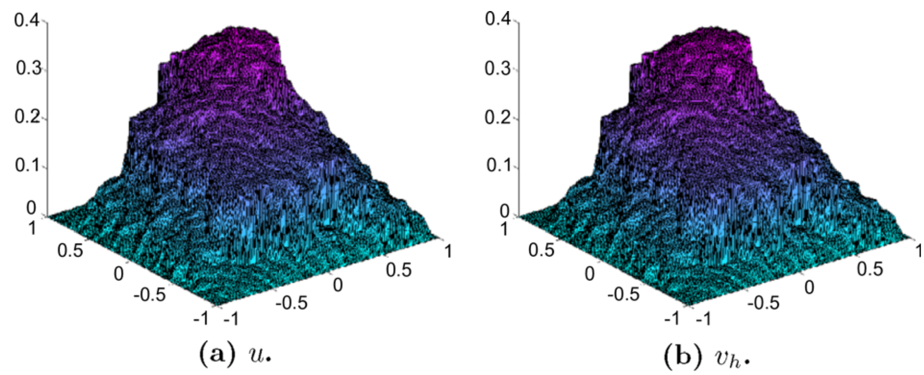

Fig. 4. u computed with *dof* 261121 and v_h computed with *dof* 9 at time 1, they are interpolated on a coarser mesh in order to have a clear picture.

Table 7
Example 4.3, numerical errors for $g = 1$

dof_f	dof_c	L^1	L^∞	L^2	H^1
65,025	9	0.0750	0.0777	0.0729	0.1528
	49	0.0301	0.0351	0.00298	0.0779
	225	0.0135	0.0147	0.0133	0.0333
261,121	9	0.0752	0.0779	0.0731	0.1533
	49	0.0302	0.0345	0.0299	0.0782
	225	0.0131	0.0145	0.0130	0.0329

Table 8
Example 4.3, numerical errors for modified source

dof_f	dof_c	L^1	L^∞	L^2	H^1
65,025	9	0.0429	0.1580	0.0505	0.4065
	49	0.0261	0.0965	0.0324	0.3030
	225	0.0185	0.0879	0.0226	0.2718
261,121	9	0.0491	0.1189	0.0578	0.4259
	49	0.0263	0.0969	0.0324	0.2780
	225	0.0178	0.1139	0.0221	0.2474

with $\sigma = 0.05$, $T(t) = T_1(t)T_2(t)$

$$T_1(t) = \sum_1^{10} 2\frac{1-(-1)^k}{k\pi}\sin(2k\pi t), \tag{4.5}$$

and $T_2(t) = \operatorname{erfc}(8(t-0.5))$, erfc is the complementary error function. We use this source term to emulate a source acting around the origin before $t = 0.5$, then suddenly decays. See Fig. 5 for $T(t)$ in $(0, 1)$.

In fact, our future goal is to simulate the response of an explosion, usually this is done with a so-called Ricker function [6], i.e., $g(x, y, t) = \delta_0(x - x_s, y - y_s)R(t)$ with

$$R(t) = (1 - 2\pi^2(f_0t-1)^2)\exp(-\pi^2(f_0t-1)^2], \tag{4.6}$$

where δ_0 is the Dirac function and f_0 is called the central frequency of the source wavelet. It is clear that Ricker function does not belong

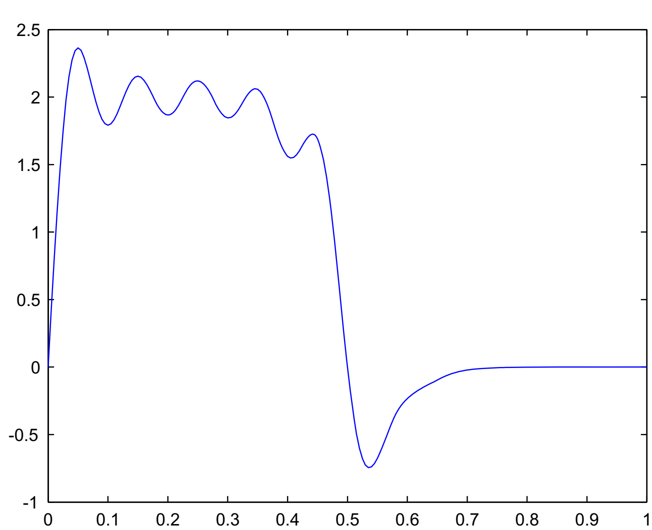

Fig. 5. $t \to g(0, t)$.

to $L^2(\Omega_T)$, our analysis does not apply and numerical experiment failed in this case. Therefore, we would like to test the above modified source term first.

Numerical errors for this modified source are given in Table 8. The errors are acceptable but not so good as $g = 1$. Possible solutions include the adaptive integration in time and adaptation in space around the source.

5. Conclusion and further remarks

From above analysis and numerical examples, we observe that good numerical approximations can be obtained with much fewer degrees of freedom for acoustic wave equation with heterogeneous coefficients, even for the cases which do not satisfy the Cordes condition. Compared with the multi-scale finite element method which compute the basis locally, our method has much better accuracy, especially for problems with strong non-local effects.

As it has been done in [29], once one understand that the key idea for the homogenization of (1.1) lies in its higher regularity properties with respect to harmonic coordinates one can homogenize (1.1) through a different numerical method (such as a finite volume method).

Moreover, it could be observed that one could use any set of n linearly independent solutions of (1.1) instead of the harmonic coordinates. The key property allowing the homogenization of (1.1) lies in the fact that if the data (right hand side and initial values) has enough integrability then the space of solutions is at small scales close in H^1 norm to a space of dimension n. Thus, once one has observed at least n linearly independent solutions of (1.1), one has seen all of them at small scales.

Write $L := -\nabla a \nabla$. L^{-1} maps $H^{-1}(\Omega)$ into $H^1_0(\Omega)$, it also maps $L^2(\Omega)$ into V a subspace of $H^1_0(\Omega)$. V is close in H^1 norm to a space of dimension n (the dimension of the physical space Ω) in the following sense.

Let $\mathscr{T}_h$ be a triangulation of $\Omega \subset \mathbb{R}^n$ of resolution h (where $0 < h < \mathtt{diam}(\Omega)$). Let Λ set of mappings from $\mathscr{T}_h$ into the unit sphere of $\mathbb{R}^{n+1}$ (if $\lambda \in \Lambda$ then λ is constant on each triangle $K \in \mathscr{T}_h$ and $\|\lambda(K)\| = 1$), then

$$\sup_{v_1,v_2,\dots,v_{n+1}\in V}\ \inf_{\lambda\in\Lambda} \frac{\left\|\sum_{i=1}^{n+1}\lambda_i v_i\right\|_{H_0^1(\Omega)}}{\sum_{i=1}^{n+1}\|\nabla a\nabla v_i\|_{L^2(\Omega)}} \leqslant Ch. \tag{5.1}$$

Eq. (5.1) is saying that any $n+1$ elements of V are (at an h approximation in H^1 norm) linearly dependent. Recall that $n+1$ vectors are linearly dependent in a linear combination (with non null coefficients) of these vectors in the null vector. In (5.1) the linear combination of the $n+1$ vectors is at relative distance of order h (resolution of the triangulation) from 0.

We notice that some recent results using global information [1,23,22] are formulated in a partition of unity framework [8]. In this case, $\{1,F_1,\dots,F_n\}$ can be used to construct the local approximation space.

Acknowledgement

We thank the anonymous referee for valuable comments on our draft.

References

[1] J.E. Aarnes, Y. Efendiev, L. Jiang, Mixed multiscale finite element methods using limited global information, Multiscale Model. Simulat. 7 (2) (2008) 655–676.
[2] G. Alessandrini, V. Nesi, Univalent σ-harmonic mappings: connections with quasiconformal mappings, J. Anal. Math. 90 (2003) 197–215.
[3] G. Allaire, R. Brizzi, A multiscale finite element method for numerical homogenization, Multiscale Model. Simulat. 4 (3) (2005) 790–812 (Preliminary version: internal report, no. 545, CMAP, Ecole Polytechnique, July 2004).
[4] P.W. Anderson, Absence of diffusion in certain random lattices, Phys. Rev. 109 (1958) 1492–1505.
[5] J.P. Aubin, Behavior of the error of the approximate solutions of boundary value problems for linear elliptic operators by Galerkin's and finite difference methods, Ann. Scuola Norm. Sup. Pisa 21 (1967) 599–637.
[6] M. Azaiez, B.F. Belgacem, H. El Fekih, M. Ismail, Numerical simulation of the wave equation with discontinuous coefficients by nonconforming finite elements, Numer. Methods Partial Diff. Eq. 15 (6) (1999) 637–656.
[7] I. Babuška, G. Caloz, J.E. Osborn, Special finite element methods for a class of second order elliptic problems with rough coefficients, SIAM J. Numer. Anal. 31 (4) (1994) 945–981.
[8] I. Babuška, J.M. Melenk, The partition of unity method, Int. J. Numer. Methods Engrg. 40 (4) (1997) 727–758.
[9] A. Bamberger, R. Glowinski, Q.H. Tran, A domain decomposition method for the acoustic wave equation with discontinuous coefficients and grid change, SIAM J. Numer. Anal. 34 (2) (1997) 603–639.
[10] N. Berglund, Perturbation theory of dynamical systems, 2001. arXiv:math/0111178v1 [math.HO].
[11] J.H. Bramble, S.R. Hilbert, Estimation of linear functionals on Sobolev spaces with application to fourier transforms and spline interpolation, SIAM J. Numer. Anal. 7 (1970) 112–124.
[12] S. Campanato, Un risultato relativo ad equazioni ellittiche del secondo ordine di tipo non variazionale, Ann. Scuola Norm. Sup. Pisa (32) (1967) 701–707.
[13] Y.R. Efendiev, T.Y. Hou, X.H. Wu, Convergence of a nonconforming multiscale finite element method, SIAM J. Numer. Anal. 37 (3) (2000) 888–910 (Electronic).
[14] L. Evans, Partial Differential Equations, Graduate Studies in Mathematics, vol. 19, American Mathematical Society, 1997.
[15] C.L. Farmer, Upscaling: a review, Numer. Methods Fluids 40 (2002) 63–78.
[16] J. Fish, A. Wagiman, Multiscale finite element method for a locally nonperiodic heterogeneous medium, Comput. Mech. 12 (3) (1993) 164–180.
[17] M.S. Floater, One-to-one piecewise linear mappings over triangulations, Math. Comput. 72 (242) (2003) 685–696.
[18] V.A. Garanzha, Variational principles in grid generation and geometric modelling: theoretical justifications and open problems, Numer. Linear Algebra Appl. 11 (2004) 535–563.
[19] K. Höllig, Finite Element Methods with B-Splines, Frontiers in Applied Mathematics, vol. 26, Society for Industrial and Applied Mathematics (SIAM), Philadelphia, PA, 2003.
[20] K. Höllig, U. Reif, J. Wipper, Weighted extended B-spline approximation of Dirichlet problems, SIAM J. Numer. Anal. 39 (2) (2001) 442–462.
[21] T.Y. Hou, X.H. Wu, A multiscale finite element method for elliptic problems in composite materials and porous media, J. Comput. Phys. 134 (1) (1997) 169–189.
[22] L. Jiang, Y. Efendiev, V. Ginting. Global multiscale methods for acoustic wave equations with continuum spatial scales, submitted for publication.
[23] L. Jiang, Y. Efendiev, V. Ginting, Multiscale methods for parabolic equations with continuum spatial scales, Discrete Contin. Dyn. Syst. Ser. B. 8 (4) (2007) 833–859.
[24] W. Kohler, G. Papanicolaou, B. White, Localization of low frequency elastic waves, Stochastic Models in Geosystems (Minneapolis, MN, 1994), IMA Vol. Math. Appl., vol. 85, Springer, New York, 1997. pp. 209–217.
[25] A. Maugeri, D.K. Palagachev, L.G. Softova, Elliptic and Parabolic Equations with Discontinuous Coefficients, Mathematical Research, vol. 109, Wiley VCH, 2000.
[26] P. Ming, X. Yue, Numerical methods for multiscale elliptic problems, J. Comput. Phys. 214 (2006) 421–445.
[27] F. Murat, L. Tartar, H-convergence, Topics in the Mathematical Modelling of Composite Materials, Programming Nonlinear Differential Equations Application, vol. 31, Birkhäuser Boston, Boston, MA, 1997. pp. 21–43.
[28] H. Owhadi, L. Zhang, Homogenization of parabolic equations with a continuum of space and time scales, SIAM J. Numer. Anal. 46 (1) (2007) 1–36. Available from: arxiv:arXiv:math/AP/0512504.
[29] H. Owhadi, L. Zhang, Metric based upscaling, Commun. Pure Appl. Math. 60(5) (2007) 675–723. Available from: arxiv:arXiv:math/NA/0505223.
[30] P. Sheng, Introduction to Wave Scattering, Localization and Mesoscopic Phenomena, Academic, San Diego, 1995.
[31] W.W. Symes, Mathematics of Reflection Seismolgy, 1998. (Lecture notes, available at <http://www.trip.caam.rice.edu/txt/tripinfo/other_list.html>).
[32] L. Tartar, Homogénéisation et compacité par compensation, in: Séminaire Goulaouic–Schwartz (1978/1979), p. Exp. No. 9, 9. École Polytech., Palaiseau, 1979.
[33] T. Vdovina, S.E. Minkoff, O. Korostyshevskaya, Operator upscaling for the acoustic wave equation, Multiscale Model. Simulat. 4 (4) (2005) 1305–1338.